DOI 10.1007/s10812-024-01674-3
Journal of Applied Spectroscopy, Vol. 90, No. 6, January, 2024 (Russian Original Vol. 90, No. 6, November–December, 2023)

RESISTANCE OF ACETYL-, FORMYL-, AND METHOXY-PHENYLBORONIC ACIDS TO BOROXINE FORMATION AND THEIR EMPLOYMENT IN FLUORIDE DETERMINATION OF DENTAL FORMULATIONS AND BEVERAGES BY FLUORESCENCE QUENCHING

Emrah Kilinc

UDC 535.37;535.34

Phenylboronic acids (PBAs) form stable complexes with fluoride. The effect of type (methoxy-, formyl-, and acetyl-) and position (ortho-, meta-, and para-) of electron-donating substitutions on the hydrolytic stability and acidity of PBAs, as well as their spectroscopic and physicochemical properties and their usage in spectrofluorimetric fluoride determination, were investigated. Thermal stabilities, relative predisposition, and resistance to dehydroboronation of related PBA isomers were investigated in detail and compared with the use of thermogravimetric analysis and differential scanning calorimetry profiles. Dehydroboronation reaction leads to the synthesis of related new cyclic anhydric forms — specifically named boroxines — which are clearly distinguished by Fourier transform infrared spectroscopy. PBAs were used for the complexation of fluoride for spectrofluorimetric fluoride determination in dental formulations [toothpastes (TPs) and mouth rinses (MRs)] and beverages [mineral waters (MiWs)]. Determination was done by fluorescence quenching of PBAs in response to increasing fluoride concentration. The regression equation was $y = -15.336x + 983.17$ ($R^2 = 0.9931$), *and was linear in the 1.4–3.0-mM range. Determinations were performed with relative errors (%) in a range of –5.60 to +1.23, –2.01 to +5.69, and –4.16 to +2.54 for MRs, TPs, and MiWs, respectively, relative to fluoride levels of commercial samples. Chemometric analyses (cluster analysis, CA, principal component analysis, PCA) were performed on the same real samples. Raw fluorescence data was investigated by PCA to check their significance in chemometric discrimination. Dendograms and score plots successfully discriminated samples in related groups. This is the first demonstration of spectrofluorometric fluoride determination based on the quenching of related isomers of PBAs thus far, also the potential of raw fluorescence data of these PBAs for chemometric discrimination studies on related pharmaceutical samples was highlighted for the first time.*

Keywords: *Fourier transform infrared spectroscopy, differential scanning calorimetry, thermogravimetric analysis, fluorescence quenching, phenylboronic acids, boroxines, chemoinformatics.*

Introduction. In recent years, growing interest has started focusing on the chemistry of boronic acids (BAs) due to their wide spectrum of usage in engineering and material science, organic chemistry, analytical chemistry, and even in medicinal or biological sciences [1–7]. BAs display Lewis acidic behavior and tend to adopt electrons and become an electrophile. Increasing acidity has its own possible drawback, namely, easier dehydroboronation [8]. Phenyl boronic acids (PBAs) also go under dehydration reaction in time, naturally occurring especially in heat-including procedures (e.g., spray drying) or via extended storage at room temperature [9]. This dehydration reaction results in the generation of related cyclic anhydrates: boroxines (BXNs) [10]. Thus, thermal and hydrolytic stability should be investigated by thermogravimetric analysis (TGA) and differential scanning calorimetry (DSC). Heat-generating processes of these methods contain miscellaneous endothermic reactions: melting of PBAs, evaporation of crystalline water, BXNs formation (with dehydration), melting of formed BXNs, and even fragmentation of the sample [10]. PBAs derivatives are successfully employed also in electrochemical (voltametric) and spectrofluorimetric determination of various analytes [11–24].

In the current work, we aimed firstly to examine the dependence of acidity and hydrolytic stability of the investigated PBAs on different substitutions, due to a lack of data on such isomers. DSC and TGA profiles were recorded for *ortho*-, *meta*-, and *para*-isomers of methoxy-, formyl-, and acetyl-PBAs to check their sensitivity to dehydration (BXNs). FTIR is

Ege University, Faculty of Pharmacy, Analytical Chemistry Department, Bornova Izmir, Turkey; email: emrah.kilinc@ege.edu.tr; kilince@gmail.com. Abstract of article is published in Zhurnal Prikladnoi Spektroskopii, Vol. 90, No. 6, p. 969, November–December, 2023.

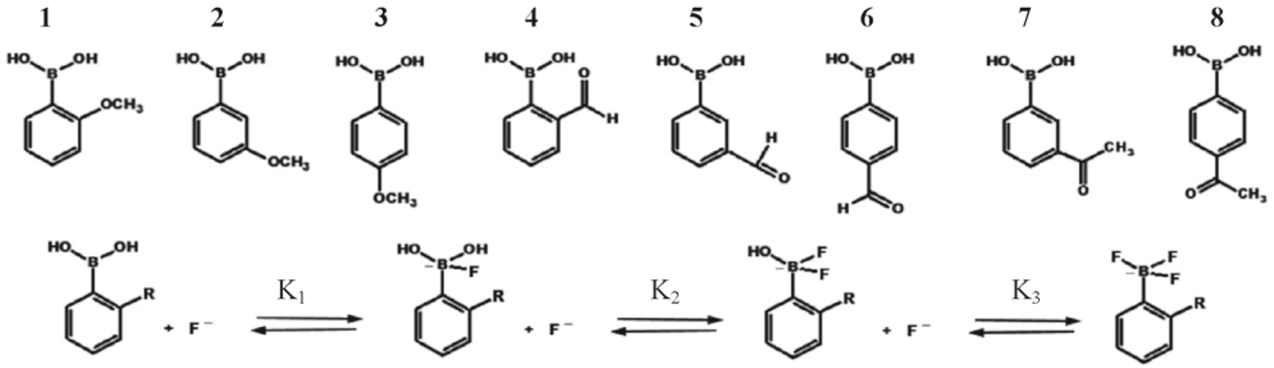

Fig. 1. Numbering and structures of compounds; *ortho*- (**1**), *meta*- (**2**), and *para*- (**3**) methoxyphenyl-BAs, *ortho*- (**4**), *meta*- (**5**), and *para*- (**6**) formylphenyl-BAs, *meta*- (**7**) and *para*- (**8**) acetylphenyl-BAs. Proposed reaction scheme for fluoride complexation of BAs, for quantification.

useful as specific FTIR signals selectively correspond to nonconjugated functional groups of BAs [25, 26] and they diminish during BXN formation. FTIR spectra were recorded for *ortho*-, *meta*-, and *para*-isomers of methoxy- (**1**–**3**), formyl- (**4**–**6**), and acetyl- (**7**, **8**) PBAs (Fig. 1). Additionally, the pK_α of BAs was determined by spectrophotometric and potentiometric methods.

The second aim was to investigate the use of PBAs for selective spectrofluorimetric determination of fluoride, based on the fluorescence quenching of PBAs upon complex formation with fluoride. Thus, compounds **1**–**8** can be used for the determination of fluoride in pharmaceutical formulations (MRs and TPs) and beverages (MiWs).

The final aim was the chemometric analysis of raw fluorescence data by principal component analysis (PCA), and cluster analysis (CA) for chemometric discrimination of samples. Raw data was converted to text format, reduced and transposed prior to PCA analysis. Score plots displayed significant discrimination of entire real samples according to the fluoride content or commercial brand. CA was also performed on finalized data and the resulting dendrograms displayed separate groups clearly, supporting PCA findings. To our best knowledge, fluorescence-quenching determination of fluoride with methoxy-, formyl-, and acetyl-PBAs isomers was demonstrated for the first time in pharmaceutical formulations and beverages. Chemometric investigation of raw fluorescence-quenching data by PCA, and CA was performed and discrimination of pharmaceutical samples and beverages was achieved for the first time. Due to the lack of data on hydrolytic stability, spectroscopic and physicochemical study of PBAs, the current manuscript will make a contribution to the literature.

Materials and Methods. 2-, 3-, and 4-isomers of formyl-PBAs (L13333, L14024, and L134429), methoxy-PBAs (L145565, L13816, and L08104), and 3-, 4-isomers of acetyl-PBAs (L15406, L15405) were obtained from Alfa Aesar. Sodium hydroxide was from Sigma-Aldrich (06203), methanol was from Merck KgaA (1.06007.2500). The ultrapure water used had TOC levels of <10 ppb and a total ion resistance level of >18.2 MΩ·cm. Membrane filters (0.45 μm) were obtained from Agilent (5185-5833).

Bandelin Sonorex RK 52 (240W) ultrasonic bath, Hanna HI-5222 pH meter, and A&D HR120 analytical balance were used. Ultrapure water system was ELGA Classic UV MK2. Ocean Optics USB4000-FL spectrofluorimeter and Spectra Suite software, USB-LS-450 LED light source and CUV-FL-DA cuvette holder were used. Thermo Scientific Evolution Array UV-Vis spectrophotometer and Vision Collect software, Perkin Elmer Spectrum100 FT-IR Spectrometer with Spectrum software and UATR Accessory for Spectrum Two, Diamond were used. Perkin Elmer DSC6000 Differential Scanning Calorimeter and Perkin Elmer TGA4000 Thermogravimetric Analyzer were used with Puris software.

PBAs (10^{-2} M) and NaF (5–100 mM) solutions were prepared and stored at 4^{o}C up to 36 h. TPs, MRs, and MiWs were from local markets (Tables 1–3). Two millimeters of MRs were added on Accubond^{II} ODS-C18 SPE cartridges at a 5-μL/min flow rate. A total of 1.0 g TPs was sonicated for 10 min in 2 mL of ultrapure water, suspension was transferred to SPE cartridges (same flow rate). One millimeter of MiWs was mixed with 1mL of ultrapure water and added to SPE cartridges (same flow rate), while 1.5 mL of extracts were mixed with 1.5 mL of 0.05 M phosphate buffer (pH 7.4) prior to measurement.

NaOH titrant was used, the UV-Vis spectrum (200–600 nm) and pH of the PBA solution were acquired. Spectrophotometric (or potentiometric) pK_α were predicted by Henderson-Hasselbach equation placed in OriginPro 2022 software.

TABLE 1. Spectrofluorimetric Data for Fluoride Contents of Commercial Mouthrinses (MRs). Experimental Conditions as in Spectrofluorimetric Experiments Subsection

Sample No.	Trade mark/Company	Date of production/ Batch No.	Declared fluoride content, ppm/μM	Sampled volume, mL	Determined fluorescence intensity (Fl)	Determined fluoride content, ppm/μM	%Relative error
1	Sensodyne Gentle Mouthrinse	EXP 290610/ BN 300108	230 ppm (5472.23 μM)	1 mL	6197.7	5539.54 μM (232.83 ppm)	+1.23
2	Colgate Plax Multi Protection (Cool Mint Mouthwash)	11.03.2009/ 9070CHG11C	115 ppm (2736.12 μM)		13,118.9	2617 μM (109.99 ppm)	–4.36
3	Colgate Plax Overnight (Overnight Protection Miuthwash)	08.01.2009/ 9008CHG11C	115 ppm (2736.12 μM)		13,292.1	2582.9 μM (108.56 ppm)	–5.6
4	Oral-B Advantage Mouth Rinse	8262108571/ EXP 09 2011	*		12,910.6	2659.23 μM (111.76 ppm)	**

*Fluoride content not declared on package.

**Not detectable due to missing fluoride content declaration.

Emission spectrums (350–1050 nm) were recorded (λ_{ex} = 280 nm). Fluorescence quenching occurred with increasing fluoride levels. The dark spectrum was stored using a blank sample. Successive pH values 2.1, 3.6, 5.5, 8.7, and 10.7 (using 0.05-M acetate/phosphate buffers and methanol, 50–50%, v/v) were studied.

A 3.0-mg sample was placed in an FTIR universal UATR Accessory in the 650–4000 cm^{-1} wave number range. For DSC, a 4.0-mg sample was placed in hermetically sealed aluminum pans. The heating-cooling-heating (HCH) cycle was in the 0–225°C range (5°C/min ramping rate-Rr). A 2.0-mg sample was placed in aluminum pans for TGA. The HCH cycle was in the 30–300°C range (10°C/min Rr).

Raw spectroscopic data of each sample was imported in text format, stored and saved in separate Excel files. After which the entire folder was transferred to Minitab software (v.17.1.0) in Excel format where the imported data went through a data reduction (or regulation) process — by subtracting the mean from each data value and dividing them by the standard deviation (SD). Later columns of reduced data were transposed by converting all columns to rows. Finally, principal component analysis (PCA) was performed on the reduced and transposed data, after which the scree plot, score plot, and loading plots were obtained for the chosen number of principal components. Simultaneously, a dendrogram plot was obtained by cluster analysis.

Results and Discussion. Three isomers (*ortho*-, *meta*-, and *para*-) of methoxy- (**1**, **2**, and **3**) and formyl- (**4**, **5**, and **6**) PBAs, and two isomers (*meta*- and *para*-) for acetyl-PBAs (**7** and **8**) (Fig. 1) were investigated. Hydrolytic stability (DSC, TGA), acidity, and spectroscopic (FTIR) characterization were performed for PBAs, prior to fluoride determinations. There are a few reaction schemes for the fluoride complexation of PBAs [27–30]. Among these, the reaction scheme based on three subsequent subreactions, where three moles of fluoride are complexed by a BA group, is widely acknowledged and cited [29–31], as we also suggest in Fig. 1.

The pK_α values obtained with potentiometric titrations are in harmony with Lewis acid behavior. When an electronegative group approaches the BA structure of the phenyl ring, the total structure becomes more acidic because of the delocalization of the boron electrons, which is obvious when the *orto*- and *para*-isomers are compared. The pK_α values calculated from photometric titrations for *orto*-, *meta*-, and *para*-isomers were 9.0, 8.7, and 9.3 for **1**, **2**, and **3**, respectively, whereas the same pK_α values were 7.3, 7.7, and 7.5 for **4**, **5**, and **6**, respectively. Regarding acetyl-PBAs (**7** and **8**) 8.0 and 7.7 were the pK_α values determined. Representative experimental photometric titration spectrums and related graphs of **1** are provided in Fig. 2.

Compound **1** displays a descending absorption at 220 nm with the formation of a new species causing formation of an isosbestic point specifically at 210 nm. Decreasing absorption is displayed at 275 nm by **1**, while the ascending absorption

TABLE 2. Spectrofluorimetric Determination of Fluoride Levels in Commercial Toothpastes (TPs). Experimental Conditions as in Voltammetric Experiments Subsection

Sample No.	Trade mark/ Company	Batch No.	Declared fluoride content, ppm/μM	Sampled mass, g	Determined fluorescence intensity (Fl)	Determined fluoride content, μM	% Relative error
5	Theramed 2 in 1 (toothpaste + mouth wash) original	0816190802	1450 ppm (34,498.84 μM)	1.07	1015.6	33,805.4	–2.01
6	Theramed Titane Fresh	0819190402		1.01	1009.2	34,019.3	–1.39
7	Ipana 3 dimension whiteness	9084R4	3200 ppm (76,135.37 μM)	1.10	434.6	79,005.6	+3.77
8	Signal carbonate	0506032	1450 ppm (34498.84 μM)	1.07	969.5	35,413.1	+2.65
9	Signal green apple	B0452P151107		1.02	960.5	35,744.3	+3.61
10	Signal experience	BBN0016		1.04	961.1	35,723.5	+3.55
11	Sensodyne Pronamel	200209 L1		1.03	965.1	35,575.2	+3.12
12	Colgate Total	281123	1400 ppm (33,309.22 μM)	1.05	1027.2	33,422.5	+0.34
13	Ipana healthy smiles	G3017R70403	3200 ppm (76,135.37 μM)	1.07	447.8	76,660.7	+0.69
14	Oral-B Stages	8287L2	500 ppm (11,896.15 μM)	1.05	2859.4	12,006.8	+0.93
15	Ipana Kids	9079L5	1100 ppm (26,171.53 μM)	1.08	1308.5	26,236.9	+0.25
16	Sanino original arctic ice blast of freshness	042009001	1450 ppm (34,498.84 μM)	1.06	941.6	36,461.8	+5.69
17	Sanino original max protect multiminerals	042009012		1.00	955.7	35,923.6	+4.13
18	Sanino junior extra protection	102008009	1100 ppm (26,171.53 μM)	1.04	1269.7	27,184.4	+3.87

trend, along with the formation of a new species, makes an isosbestic point specifically at 265 nm. When absorbance of **1** at 220 nm is plotted versus absorbance at 262 nm a linear graph is obtained (Fig. 2b). Thus, verification of the model of a single equilibrium is achieved, based on this data. In Fig. 2c, absorbance variation at 220 nm versus pH is plotted, and a major decay is visible in the 9.1 to 9.6 pH range. Maximum fall-off in absorption and slowdown in absorption descension become obvious when the second derivation of absorbance (262 nm) over titrant volume (d^2A/d^2V) is plotted versus medium pH (Fig. 2d). As can be seen, when d 2A/d 2V is plotted versus pH, a derivation curve is obtained where significant decrease and increase trends are displayed for the absorbance at 220 nm at pH 9.2 and 9.4, respectively. Sporzynski et al. [8] have recently focused on hydrolytic stability and acidity of a group of 20 PBAs. They have provided titration and species distribution graphs, and data on pK_α determination and predictions for fluorinated PBAs. They have also provided photometric titration

TABLE 3. Spectrofluorimetric Quantification of Fluoride Concentrations of Commercial Beverages (Mineral Waters). Experimental Conditions as in Voltammetric Experiments Subsection

Sample No.	Trade mark/ Company	Date of production/ Batch No.	Declared fluoride content, ppm/μM	Sampled volume, mL	Determined fluorescence intensity (Fl)	Determined fluoride content, ppm/μM	% Relative error
1	Uludag Dogal Mineralli Su	11.06.2009 15:51	1.30 ppm = 30.93 μM	1 mL	1,105,349.6	1.305 ppm (31.06 μM)	+0.43
2	Kula Dogal Maden Suyu	11.05.2009	0.39 ppm = 9.28 μM		3,861,885.4	0.373 ppm (8.89 μM)	–4.16
3	S. Pellegrino Dogal Maden Suyu	10.2008 18 L7296087026	0.50 ppm = 11.89 μM		2,823,368.5	0.511 ppm (12.16 μM)	+2.294
4	Turk Kizilayi 1868 Dogal Mineralli Su	22.05.2009 05:03	0.81 ppm = 19.27 μM		1,774,271.9	0.84 ppm (19.35 μM)	+0.420
5	Kristal Dogal Mineralli Su	16.05.2009 13:02	0.56 ppm = 13.32 μM		2,513,335.4	0.57 ppm (13.66 μM)	+2.543
6	Sirma Dogal Zengin Mineralli Su	30.05.2009 20:48	1.40 ppm = 33.31 μM		1,033,478.6	1.39 ppm (33.22 μM)	–0.28

spectrums for 2,5-difluorinated and 2,3,6-trifluorinated PBAs, whose absorption alterations, in the 230–280 nm region, form an isosbestic point specifically at 266 nm. Adamczyk-Woźniak et al. [32] focused on the acidity of 1,3-phenylene-di-BA. Data of pK_α determinations, potentiometric and spectrophotometric titration graphs, and distribution diagrams were provided. In the supplements section [32], spectrophotometric titration curves of the pH range of 5.5–11.5 were provided. An isosbestic point at 262 nm was visible with successive additions of the NaOH titrant. The UV-Vis data have been investigated, focusing on absorbance change at 274 nm versus pH, using titration graphs and software calculations. In our paper [33], we also investigated hydrolytic stability, and provided potentiometric and photometric titration curves for *orto*-, *meta*-, and *para*-hydroxy-isomers of PBAs. These papers [8, 32, 33] are in accord with the current manuscript.

For the studied isomers (**1**–**8**), harmonious trends were observed regarding data of spectrophotometric and potentiometric titrations, as differences in the pK_α results did not exceed 0.1 units. Potentiometric titration curves for **5** are displayed based on experimental findings (dots) and calculation (red line). This approach is based on absorption change versus pH. Experimental and predicted data were in good harmony. These titration curves again confirm the presence of a single-step reaction equilibrium, as initially confirmed in Fig. 3a. A related pK_α value of **5** is calculated as 7.4 using the titration curve, which is similar to 7.7 in [29]. Software calculation of pK_α was performed with the use of the Henderson–Hasselbach equation in OriginPro 2022 software. The pK_α prediction of the software resulted in 7.8 ± 0.5, which is sparingly far from the experimental result of 7.4. There is commercial software used for calculating (predicting) pK_α values of various substances [27–29].

Regarding pK_α calculations, there is no paper focusing on methoxy-, formyl-, or acetyl-PBAs isomers. There are a few papers focusing on other BA compounds. Sporzynski et al. [8] have investigated the acidity of fluorinated PBAs, especially focusing on fluorinated isomers. They have performed potentiometric and spectrophotometric titrations to determine the related pK_α. Again Sporzyński et al. [9] have both potentiometrically and spectrophotometrically determined pK_α values of *ortho*-, *meta*- and *para*-trifluoromethyl-PBAs isomers and calculated pK_α as 7.9 for the *para*-trifluoromethyl-pBA (7.39 in [29]) isomer. The experimental pK_α value was determined as 7.90 and 7.82 by potentiometric and spectrophotometric methods, respectively. Adamczyk-Woźniak et al. [32] have performed potentiometric and spectrophotometric titrations to determine p$K_{\alpha1}$ and p$K_{\alpha2}$ values for 1,3-phenylene-di-BA, and they have made predictions with OriginLab software.

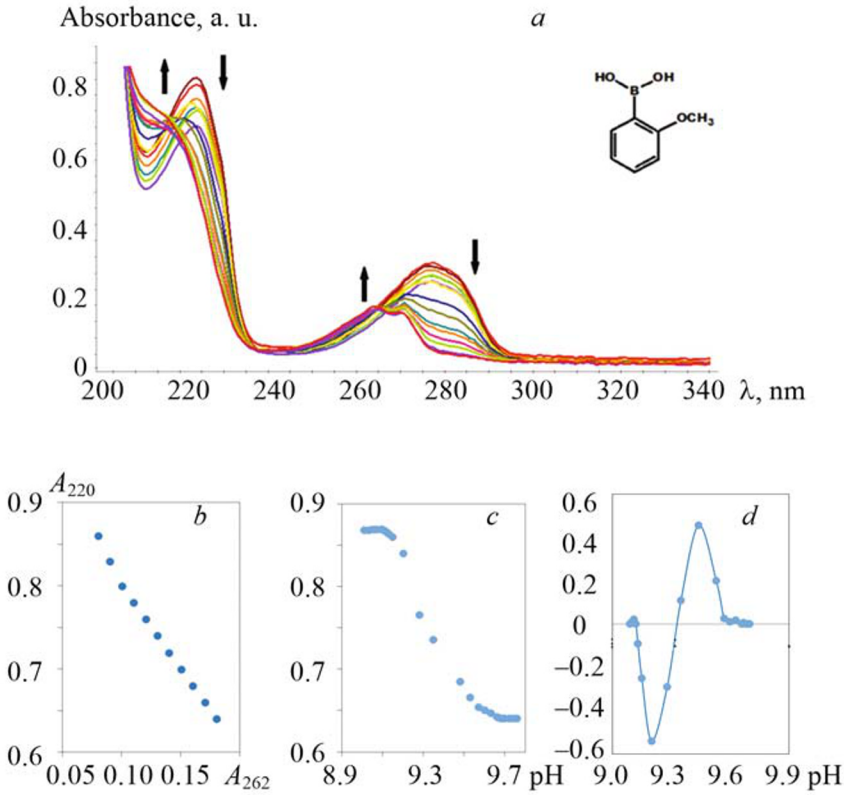

Fig. 2. Titration of 10^{-3} M **1** with 10^{-3} M NaOH (a). Graphs of dependence of absorbance at 220 nm on absorbance at 262 nm (b), on medium pH (c) and dependence of the ratio of second derivation of absorbance to second derivation of titrant volume on pH (d). Experimental conditions as in spectrophotometric pK_α.

Related p$K_{\alpha1}$ and p$K_{\alpha2}$ values were 8.26 and 9.7 (potentiometric) and 8.31 and 10.11 (spectrophotometric). In [33], we also predicted pK_αs for isomers of HPBAs using OriginLab software. Predicted values were similar to determined ones. Although these papers [8, 27–29, 32, 33] focus on other BA compounds, the predicted pK_αs were in line with the current manuscript. For the titration of **5**, a neutralization reaction is proposed (see inset in Fig. 3a) and was a single-step equilibrium that is confirmed by diagrams of linear absorbance change at 220 vs. 262 nm (Fig. 2b) and absorbance change at 220 nm vs. pH (Fig. 2c). In potentiometric (or spectrophotometric) titrations of **5**, there were four species and their concentrations in correlation with pH were summarized in the species distribution graph (SDG) provided in Fig. 3b. Sporzynski et al. [8] have provided SDG for 2,5-difluoro-PBA, similar to Fig. 5b. Adamczyk-Woźniak et al. [32] provided SDG for 1,3-phenylene-di-BA. In [33], we have also provided a similar SDG for isomers of HPBAs.

Hydrolytic stabilities of PBAs are studied by DSC and related curves for **3** and **6** (Fig. 4). DSC curves of **3** do not show any variations based on evaporation, dehydration, phase transition, degradation, or molecular reconstruction till 90°C. Events occurring in the 100–165°C range with major loss of mass occurred up to 200°C (22.3%). Neither extra mass loss nor any other events were observed in the 180–200°C range. The first endotherm (105°C) resulted from the melting of **3**. Curve shape and total mass loss (3.7%) indicate that thermal events are related to melting rather than water evaporation. BXNs are dehydration products of BAs, formed by chemical dehydration or by trimerization by ligand facilitation [8, 9, 30–33]. Thermal stability studies of BAs and BXN formation should necessarily be performed by thermal methods.

DSC and TGA were performed to identify peaks of water evaporation of **7** and **8**. TGA and DSC curves as well as the TGA profiles of entire acetyl-PBA isomers are provided in Fig. 5. Mass loss observed in the first endotherm (Fig. 5a), peak 125°C, resulted from the melting of **7**. Specific curve shapes of DSC as well as total mass loss (9.0%) indicate that observed thermal events are based on melting rather than water evaporation. Expected mass loss related to the total dehydration of acetyl-PBAs (**7**, **8**) to corresponding BXNs is 10.97%. Thus, the typical dehydration behavior of PBAs did not occur, which was

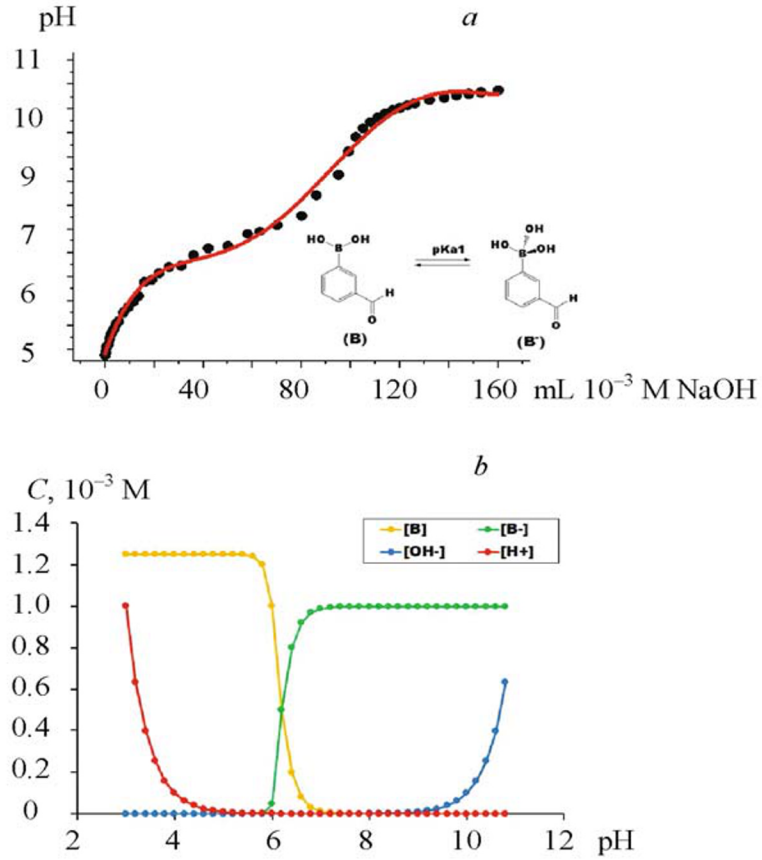

Fig. 3. Potentiometric titration curves of 10^{-3} M **5** with 10^{-3} M titrant (NaOH) (a) providing experimental (dots) and calculated (predicted) data (red line). Species distribution diagram during the titration (b). Experimental conditions as in potentiometric pK_α titration subsection.

confirmed by FTIR as BXN formation is well characterized by the disappearance of the peaks of the corresponding PBAs (e.g., 3285, 1375, 1118, and 793 cm^{-1}). For **7**, water evaporation did not occur even at higher temperatures than its melting point. Regarding TGA data, only ~2.4% of the total mass of **7** was lost by 100°C. This trend continued and a weight loss of around 10.0% was reached at 150°C (Fig. 5b). Molecular weight (MW) of acetyl-PBA isomers is 163.97 g/mol and the MW of water is 18.02 g/mole. Therefore, evaporation possibly should result in a 10.97% loss of mass of the sample, which does not match the 4% loss seen in the TGA curve (Fig. 5a).

At temperatures ≥200°C, decompositions of **7** and **8** were observed in the TGA curve (Fig. 5b), making **8** the least stable acetyl-PBA. Adamczyk-Wozniak et al. [8], investigated dehydration of *ortho*-, *meta*-, and *para*-alkoxy-PBAs and resulting BXNs. They have noted the evaporation of water and the formation of BXNs with TGA results and identified that the percentage loss of weight belongs to water (11.69%) or BXN generation by FTIR. Stella et al. [30], have studied hydrolytic stability of five PBAs isomers and BXNs. In the DSC curve, overlapping endotherms were visible. The authors concluded that the first endotherm (peak 95°C) was a result of the dehydration reaction of 4MPBA to generate its BXN. The authors also provided a TGA profile, where weight loss of 12% was seen. MWs of 4MPBA and water are 151.96 and 18.02 g/mole, respectively; therefore, evaporation should result in 11.86% loss of mass, which matches 12% loss in the TGA curve.

FTIR spectra of standards of **4**–**6** and spectra of the same standards after a routine heating–cooling–heating cycle of DSC and TGA are provided (Fig. 6). Strong and broad bands at 3285 cm^{-1} belong to ν(OH) stretching vibrations and the second strong band at around 1375 cm^{-1} belongs to ν(BO) stretching vibrations [25, 26]. BXN formation is usually confirmed by the disappearance of FTIR peaks (e.g., 3285, 1375, 1118, and 793 cm^{-1}) of PBAs. As visible in both FTIR spectra, there is no significant difference which implies that there is no evidence of BXN formation (25–200°C). Sert et

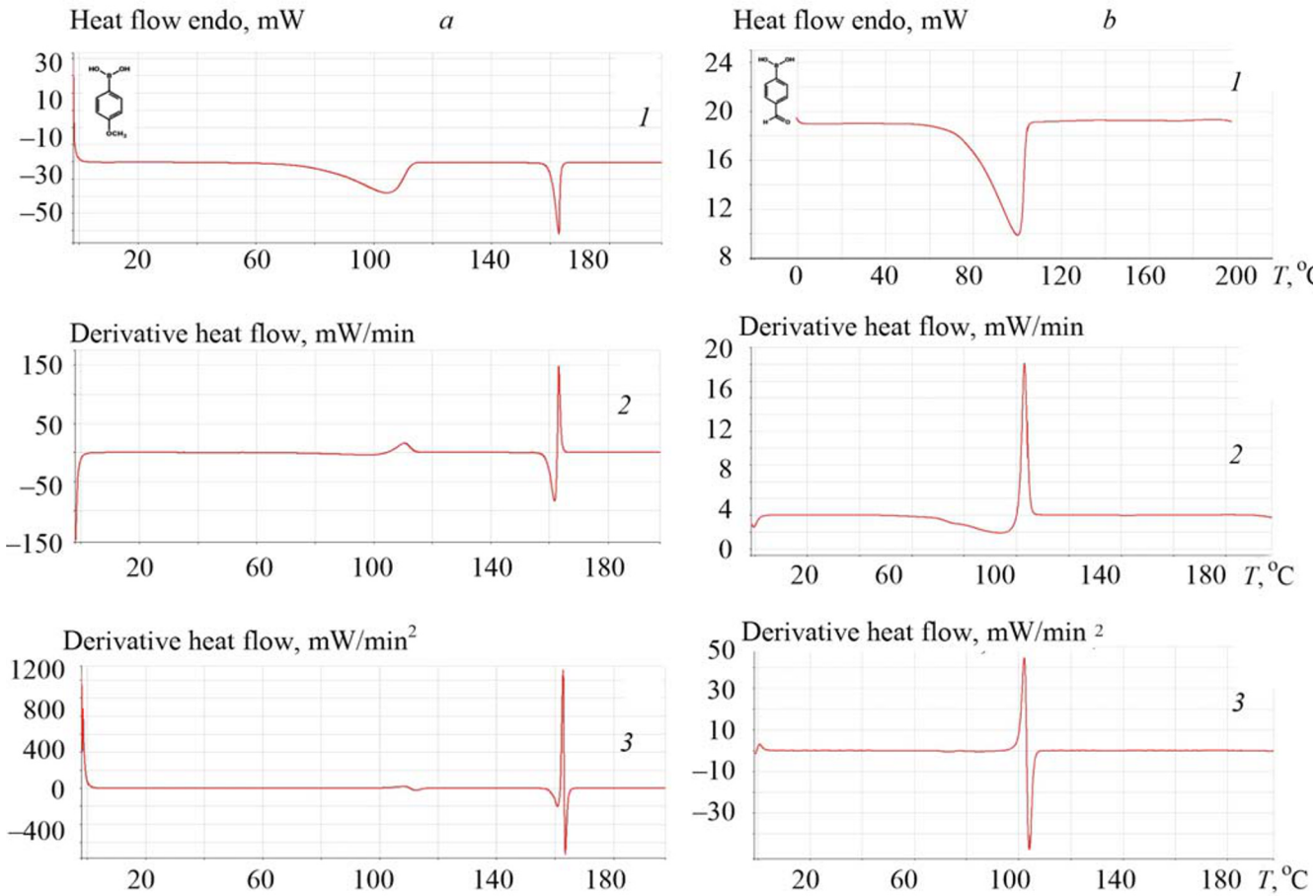

Fig. 4. The hydrolytic stabilities (DSC curves) of **3** (a) and **6** (b) under N_2 atmosphere. Heat flow endo up (mW) vs. temperature graph (*1*), first derivative of heat flow (mW/min) versus temperature curve (2), second derivative of heat flow (mW/min2) vs. temperature plot (3); 4.0 mg of sample placed in hermetically sealed aluminum pans. Heating–cooling–heating cycle was in temperature range 0–225°C (5°C/min ramping rate).

al. [25] have optimized vibrational frequencies, and related vibrational assignments for 3-hydroxy-PBA. They assigned strong and broad bands at 3380 and 1350 cm^{-1} as belonging to ν(OH) and ν(BO) stretching vibrations, respectively. FTIR spectrum and assigned frequencies are in agreement with the outcomes of the current manuscript. Dikmen et al. [26], have focused on FTIR, Raman, NMR, and XRD characterization of 2-fluoro-3-methylpyridine-5-boronic acid. They have stated that O-H stretching modes of some BAs were reported as 3480, 3467, 3465, 3443, 3440, 3425, 3410, 3397, 3280, 3276, 3249, 3175, 3108, and 3106 cm^{-1}. They have observed this band at 3350 cm^{-1} and calculated (predicted) it as 3350 cm^{-1}. Those experimental findings are compatible with the outcomes of the current manuscript. Observed FTIR bands are mainly in good harmony with the bands stated [26]. Our paper [33] has investigated hydrolytic stability and BXN formation for *orto*-, *meta*-, and *para*-hydroxy-isomers of PBAs, and BXN formation was confirmed by the disappearance of FTIR peaks at 3285, 1375, 1118, and 793 cm^{-1}, while assigned frequencies of PBAs are in harmony with this manuscript.

The dependence of the intensity of **6** on fluoride concentrations 1.4, 2.0, 2.3, 2.7, and 3.0 mM is displayed in Fig. 7. The calibration plot is based on the fluorescence quenching of **6** in an acetate buffer at pH 5.5 and is linear in the 1.4–3.0 mM range ($y = -15.336x + 983.17$, $R^2 = 0.9931$). There are some papers about the quantification of fluoride by fluorescence quenching of PBAs [11–24]. Cooper et al. [15] have performed fluoride determination with fluorescent quenching of PBAs and 2-naphthylboronic acid in 50–50% methanol–H_2O (v/v) at pH 5.5. Corresponding λ_{ex} and λ_{em} were 265 and 295 nm, respectively. Linearity was obtained for the 50–70 mM range and is relatively far from our 1.4–3.0 mM range. Arimori et al. [14] have also focused on fluoride determination by fluorescence quenching of bis(bora)calixarene in chloroform

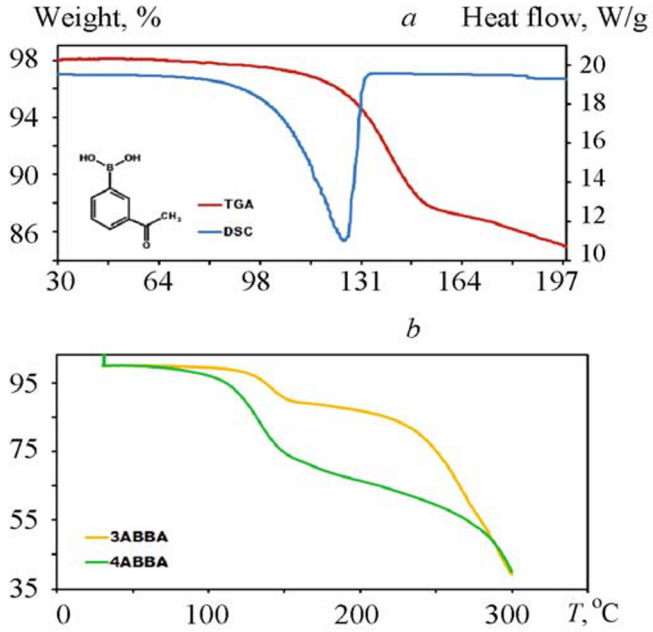

Fig. 5. DSC curve (blue) and TGA curve (red) of **7** (a). Overlay of thermograms of samples **7** and **8** (b). Experimental conditions as in DSC measurements and TGA measurements subsections.

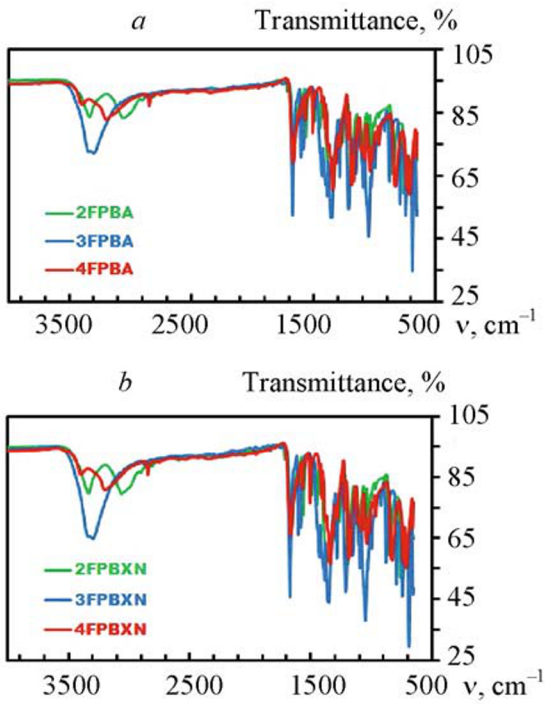

Fig. 6. FTIR spectra of pure standards of **4–6** (a) and standards after routine heating–cooling–heating cycle of DSC and TGA (b). Experimental conditions as in FTIR measurements subsection.

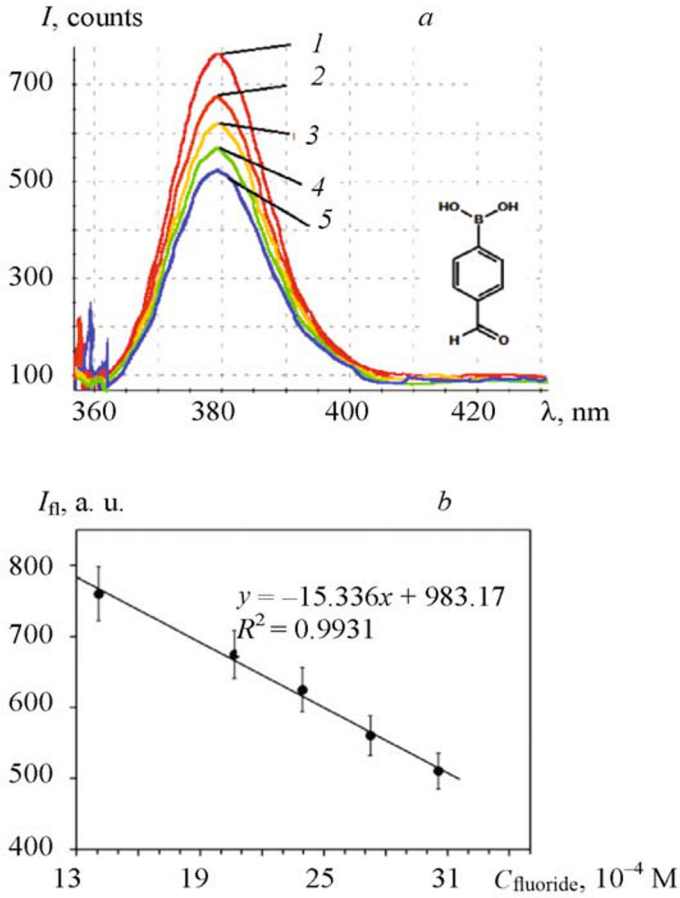

Fig. 7. Fluorescence quenching of **6** with 1400 (1), 2000 (2), 2300 (3), 2700 (4), 3000 μM (5) fluoride. Experimental conditions as in the spectrofluorimetry experiments subsection.

(λ_{ex} = 320 nm, λ_{em} = 395 nm). The linearity range was 1–10 mM, which is similar to the current study. There are papers where the pH varied in the 5.5–9.0 range [11, 12, 15, 17, 23]; in the current study, pH was optimized at 5.5, which was confirmed in [15, 23]. The literature reported some emission wavelengths for related BAs so far, such as 450 (λ_{ex} = 358 nm) [12], 390 (λ_{ex} = 325 nm) [11], 520 (λ_{ex} = 483 nm) [13] 395 (λ_{ex} = 320 nm) [14], 295 (λ_{ex} = 265 nm) [15], 464 (λ_{ex} = 298 nm) [17], and 385 nm (λ_{ex} = 295 nm) [23]. In the current study, 380 nm (λ_{ex} = 280 nm) was employed for emission monitoring. Linearity range of 1.4–3.0 mM was achieved which was wider than the 0.05–0.08 [23], and 0.005–0.06 mM [17] ranges, while narrower than the 2–10 [16], 1–10 [14], 40–280 [11], 50–300 mM [12]. Deoxygenated (argon purged) and oxygenated (air-saturated) PBA solutions had identical fluorescence spectra (not shown), which indicated that dissolved oxygen has no critical effect. Regarding the temperature (25 and 40°C) effect, again no significant difference was observed in intensities and patterns of fluorescence spectra (not shown). Additionally, the effect of possible interfering anions: bromide and iodide (66 mM) on fluorescence spectrums were investigated and no significant difference in fluorescence intensity of spectrum patterns was noticeable (not shown). In the literature, some interfering species were studied. Chloride and bromide up to 0.5 [13], 400 [11], 100 mM [12], chloride, bromide, acetate, monohydrogen phosphate, and dihydrogen phosphate up to 50 μM [17], bromide and chloride up to 6 mM [16], bromide, chloride, and iodide up to 80 μM [23] were negligible.

Limit of detection (LOD) and limit of quantification (LOQ) were calculated by LOD = $[(B_{AVE} + 3SD) - b]a^{-1}$, where B_{AVE}, SD, b, and a are baseline width average, standard deviation of baseline, intercept, and slope of calibration graph, respectively. For LOQ calculations, 10 SD was used. LOD and LOQ values were 5.66×10^{-7} M (78.07 ppb) and 4.86×10^{-7} M (67.11 ppb), respectively. LOD is lower than 5×10^{-4} [15], 10^{-3} [11, 12, 14], and 3×10^{-6}M [13], thus sensitive determinations may be possible in a range of 10–10^3 folds.

Fluoride levels in commercial MRs are given (Table 1). Related raw data is provided in Fluorescence_RAW DATA_Mouthrinses_and_Toothpastes.xlsx. Commercial MRs samples showed fluoride contents in the 115–235 ppm

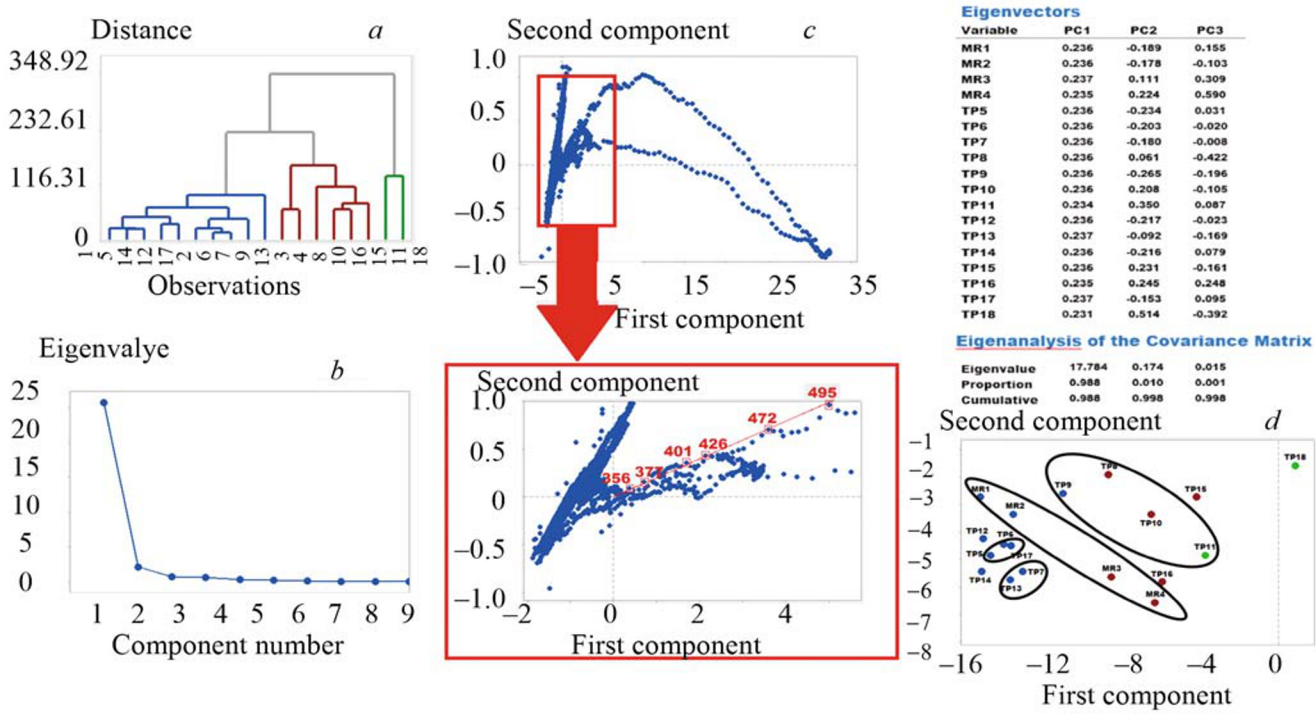

Fig. 8. Chemometric analysis of TPs and MRs, Eigenvectors/Eigenanalysis tables as well as dendrogram (a), scree plot (b), loading plot (c), and score plot (d). Experimental conditions as in chemometric.

(2.74–5.60 mM) range. Fluorescence intensities (FI) were observed as 6197.7, 13,118.9, 13,292.1, and 12,910.6 FI for MRs samples **1**, **2**, **3**, and **4**, respectively. These Fl values correspond to fluoride levels of 232.8 (5.54), 109.9 (2.62), 108.6 (2.58), and 111.76 ppm (2.66 mM). Relative to declared levels, determined concentrations own relative errors (%) of +1.23, –4.36, and –5.60% for samples **1–3**, respectively. As the fluoride content of MRs sample **4** is not declared on its commercial packing, its relative error could not be calculated. Raw experimental data is provided in Fluorescence_RAW DATA_Mouthrinses _and_Toothpastes.xlsx. Commercial TPs own fluoride content in the 500–3200 ppm range (11.9–76.1 mM). Relative errors (%) are in the –2.01 to +5.69% range (Table 2). Errors are higher than those of MRs (Table 1) and MiWs (Table 3). The most possible reason for this may be the presence of more interfering species found in TPs such as colorants, aromas, conservators. flavors, and various charged molecules, which cause TPs to be more matrix environments. Raw data are provided in Fluorescence_RAW DATA__Mineral Waters.xlsx. Fluoride levels and relative errors (%) lay in ranges of 0.373 to 1.39 ppm (8.89 to 33.22 µM) and –4.16 to +2.54%, respectively.

Chemometric analysis of TPs and MRs are summarized in Fig. 8. Eigenvectors and Eigenanalysis tables as well as dendrogram of CA, score plot, loading plot, score plot of PCA are provided. CA and PCA were performed on raw fluorescence data. The dendrogram plot distinguishes that there are three main clusters using Euclidean distances (Fig. 8a). Each cluster is displayed in a representative color and the three clusters are formed by TP1,2,5-7,9,12,14,17,13 (blue), TP3,4,8,10,15,16 (red) and TP11,18 (green), respectively. Thus, while using CA results (dendrogram) only, discrimination of MRs from TPs and discrimination of different brand TPs (same fluoride content) are not possible. On the other hand, with the use of PCA, these discriminations are successfully achieved as PCA indicated discrimination of dental formulations in groups. A trend of separation for MRs and TPs was visible with 98.8 and 99.8% of the data variability being explained by PC1 and PC1–PC2, respectively (Fig. 8b), which implies that raw fluorescence data was capable of distinguishing groups. The contribution of the remaining PCs accounted for 99.8 (PC3) and 99.9% (PC4–PC6) of total variance, respectively. Regarding the PCA score plot (Fig. 8d), dental formulation data is mainly concentrated in four significant groups, which are mainly concentrated in samples TP5,6,17 and TP8–11 and TP7,13 and MR1–4. Samples TP5,6 belong to TPs with theramed and sanino brands with 1450-ppm fluoride content, while samples TP8–11 belong to TPs of the signal and sensodyne brands with 1450 ppm fluoride. Samples MR1–4 belong to MRs, with totally different prescriptions

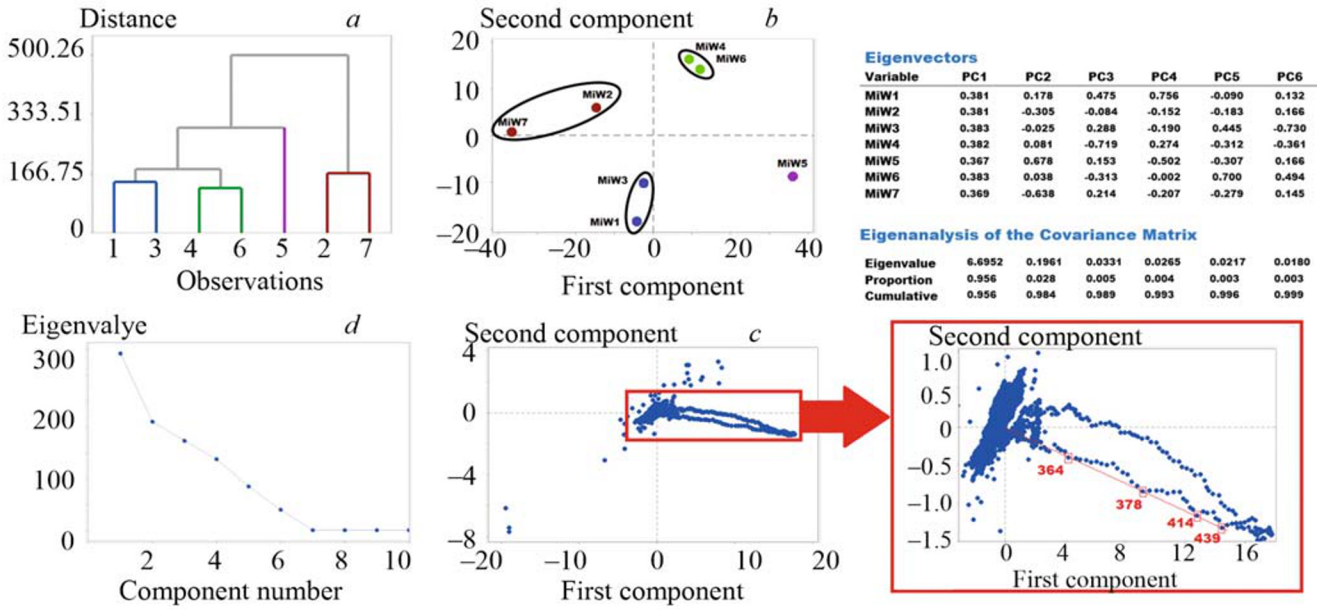

Fig. 9. Chemometric analysis of MiWs, Eigenvectors/Eigenanalysis tables as well as dendrogram (a), score plot (b), loading plot (c), and scree plot (d). Experimental conditions as in chemometric.

than TPs. Their fluoride contents are declared in the 115–230 ppm (2.74–5.47 mM) range. Samples, TP12,14–16, are not significantly related to any distinguished group on the plane (Fig. 8d). The loading plot of PCA analysis (Fig. 8c) indicates that regardless of the dental formulation's own high or low fluoride levels, fluoride contents were not necessarily associated with discrimination. The loading plot also displays the exact wavelengths where the distribution of fluorescence data exhibited noticeable variations from the general trend, such as 356, 377, 401, 426, 472, and 495 nm. The data acquired at these specific wavelengths are significant and are used for chemoinformatic tools like PCA. Alterations in orientations of TP11 and 18 on the plane may be due to the presence of other ingredients (e.g., colorants, flavors, aromas, etc.) making a contribution to separation.

In Fig. 9 chemometric analysis on MiWs is summarized. CA provided related dendrogram, while the score plot, and the loading plot as well as Eigenanalysis tables were outcomes of PCA. All these results summarize multivariate analysis performed on fluorescence quenching raw data to evaluate discrimination of MiWs between groups. CA dendrogram, clearly distinguishes that there are four main clusters using Euclidean distances (Fig. 9a). In the PCA score plot (Fig. 9b), fluorescence data of MiWs forms four significant groups, whereby MiW1–3 classifies one group, MiW4 and 6 another, while MiW2 and 7 classify in yet another group, while MiW5 stood alone. The first principal component (PC1) described 95.6% of total variance, while PC1 and PC2 together described 98.4%, which implies that raw fluorescence data may successfully be used for distinguishing groups of MiWs. The contribution of PC3–PC6 accounted for 98.9, 99.3, 99.6, and 99.9% of the total variance among MiWs, respectively (Fig. 9d). Although regardless of whether MiWs own high or low fluoride levels, fluoride contents were not necessarily associated with discrimination, but changes in orientations of MiW2 and 7 on the plane may be related to MiW2 having the least fluoride content (0.39 ppm = 9.28 µM) and MiW7 being a blank sample (no fluoride content) produced in our lab. Changes in orientations of MiW1 on the plane may be associated with the presence of other ingredients (e.g., flavors, other ions, aromas, colorants), making some contribution to the separation of groups. The loading plot (Fig. 9c) displays specific wavelengths where the distribution of fluorescence data exhibited noticeable variations from the general trend, such as the ones at 364, 378, 414, and 439 nm. The data acquired at these exact wavelengths is significant and helpful for chemoinformatic tools like PCA. Any possible effect of any other active ingredients on plane orientations, making a contribution to the separation of groups, is not explicable based on raw fluorescence quenching data this time. Thus chromatographic (LC–MS/MS) solutions are essential and would be quite helpful, but may be the subject of another study. To our best knowledge, there is no paper, focusing on the grouping and discrimination of studied samples based on PCA on raw fluorescence data; thus, no further discussion could be performed for literature comparison.

Conclusions. Hydrolytic stability and acidity of methoxy-, formyl-, and acetyl-PBAs isomers as well as spectroscopic and physicochemical properties and finally possible usage in spectrofluorimetric fluoride determinations in real samples were investigated. Related pK_α were determined by spectrophotometric and potentiometric titrations. Location of an electron-donating functional group in the aromatic ring enhances Lewis acidity of PBAs, depending on the position. TGA and DSC profiles were used to compare hydrolytic stabilities and sensitivity to dehydration, which causes the generation of cyclic anhydrides (BXNs). FTIR was used for studying the structural data of PBAs and BXNs. No significant evidence was noticeable for BXN formation in the 25–200^{o}C range. PBA isomers were employed for the selective spectrofluorimetric determination of fluoride in samples. Fluoride detection is based on the fluorescence quenching of PBAs due to complex formation with fluoride. Thus, compounds **1**–**8** can be used for fluoride determination in pharmaceutical formulations (MRs and TPs) and beverages (MiWs). Additionally, chemometric analysis was performed by CA and PCA, based on raw fluorescence data, for chemometric discrimination. To our best knowledge, the determination of fluoride by fluorescence quenching of studied PBAs was demonstrated for the first time for pharmaceutical formulations and beverages. Simultaneously, chemometric investigations were performed for the first time on raw fluorescence data for the discrimination of samples. Also, due to lack of data on hydrolytic stability, spectroscopic and physicochemical behaviours of model PBAs, we believe that the current manuscript will make a contribution to the literature.

Acknowledgments. This work was supported by National Boron Research Institute (Project No. BOREN-2008-Ç0138) and Ege University Scientific Research Projects Coordination Unit (Project No. 2008-BIL-002). The author also thanks FABAL (Pharmaceutical Sciences Research Laboratory of Faculty of Pharmacy of University of Ege, Izmir, Türkiye; https://www.fabal.ege.edu.tr) for DSC, TGA, and FTIR measurements.

REFERENCES

1. S. Pillitteri, P. Ranjan, E. V. Van der Eycken, and U. K. Sharma, *Adv. Synth. Catal.*, **364**, 1643–1665 (2022), doi: 10.1002/adsc.202200204.
2. D. G. Hall, *Chem. Soc. Rev*., **48**, 3475–3496 (2019), doi: 10.1039/c9cs00191c.
3. W. L. A. Brooks and B. S. Sumerlin, *Chem. Rev.*, **116**, 1375–1397 (2016), doi: 10.1021/acs.chemrev.5b00300.
4. R. Wang, Z. Bian, D. Zhan, Z. Wu, Q. Yao, and G. Zhang, *Dyes Pigments*, **185**, Article ID 108885 (2021), doi: 10.1016/j.dyepig.2020.108885.
5. M. P. Silva, L. Saraiva, M. Pinto, and M. E. Sousa, *Molecules*, **25**, 4323 (2020), doi: 10.3390/molecules25184323.
6. B. J. Graham, I. W. Windsor, B. Gold, and R. T. Raines, *PNAS*, **118**, e2013691118 (2021), doi: 10.1073/pnas.2013691118.
7. Y. Y. Aung, A. N. Kristanti, H. V. Lee, and M. Z. Fahmi, *ACS Omega*, **6**, 17750–17765 (2021), doi: 10.1021/acsomega.1c01352.
8. D. Zarzeczańska, A. Adamczyk-Woźniak, A. Kulpa, T. Ossowski, and A. Sporzyński, *Eur. J. Inorg. Chem*., 4493–4498 (**2017**), doi: 10.1002/ejic.201700546.
9. A. Adamczyk-Woźniak, E. Kaczorowska, J. Kredatusova, I. Madura, P. H. Marek, A. Matuszewska, A. Sporzyński, and M. Uchman, *Eur. J. Inorg. Chem.,* **2018**, 1492–1498 (2018), doi: 10.1002/ejic.201701485.
10. A. L. Korich and P. M. Iovine, *Dalton Trans.*, **39**, 1423–1431 (2010), doi: 10.1039/b917043j.
11. N. Dicesare and J. R. Lakowicz, *Anal. Biochem.*, **301**, 111–116 (2002), doi: 10.1006/abio.2001.5476.
12. R. Badugu, J. R. Lakowicz, and C. D. Geddes, *Sens. Actuators B Chem.*, **104**, 103–110 (2005), doi: 10.1016/j.snb.2004.04.119.
13. K. M. K. Swamy, Y. J. Lee, H. N. Lee, J. Chun, Y. Kim, S. J. Kim, and J. Yoon, *J. Org. Chem*., **71**, 8626–8628 (2006), doi: 10.1021/jo061429x.
14. S. Arimori, M. G. Davidson, T. M. Fyles, T. G. Hibbert, T. D. James, and G. I. Kociok-Köhn, *Chem. Commun.*, **40**, 1640–1641 (2004), doi: 10.1039/b404937c.
15. C. R. Cooper, N. Spencer, and T. D. James, *Chem. Commun*., **24**, 1365–1366 (1998), doi: 10.1039/A801693C.
16. J. M. Koskela, T. M. Fyles, and T. D. James, *Chem. Commun.*, **41**, 945–947 (2005), doi: 10.1039/B415522J.
17. W. Tan, D. Zhang, and D. Zhu, *Bioorg. Med. Chem. Lett.*, **17**, 2629–2633 (2007), doi: 10.1016/j.bmcl.2007.01.099.
18. J. K. Day, C. Bresner, N. D. Coombs, I. A. Fallis, L. L. Ooi, and S. Aldridge, *Inorg. Chem.*, **47**, 793–804 (2008), doi: 10.1021/ic701494p.
19. M. Nicolas, B. Fabre, and J. Simonet, *Electrochim. Acta*, **46**, 1179–1190 (2001), doi: 10.1016/S0013-4686(00)00694-0.
20. M. Nicolas, B. Fabre, and J. Simonet, *Chem. Commun.*, **25**, 1881–1882 (1999), doi: 10.1039/A905136H.

21. S. Sole and F. P. Gabbai, *Chem. Commun.*, **40**, 1284–1285 (2004), doi: 10.1039/B403596H.
22. M. Melami, S. Solé, C. W. Chiu, H. Wang, and F. P. Gabbai, *Inorg. Chem.*, **45**, 8136–8143 (2006), doi: 10.1021/ic060709s.
23. W. Tan, D. Zhang, Z. Wang, C. Liu, and D. Zhu, *J. Mater. Chem.*, **17**, 1964–1968 (2007), doi: 10.1039/b618183j.
24. S. Yamaguchi, S. Akiyama, and K. Tamao, *J. Am. Chem. Soc.*, **123**, 11372–11375 (2001). doi:10.1021/ja015957w.
25. Y. Sert, F. Ucun, and M. Boyukata, *Indian J. Phys.*, **87**, 113–119 (2013), doi: 10.1007/s12648-012-0202-3.
26. O. Alver and G. Dikmen, *J. Mol. Struct.*, **1108**, 103–111 (2016), doi: 10.1016/j.molstruc.2015.11.041.
27. C. Liao and M. C. Nicklaus, *J. Chem. Inf. Model.*, **49**, 2801–2812 (2009), doi: 10.1021/ci900289x.
28. C. Dardonville, *Drug Discov.*, **27**, 49–58 (2018), doi: 10.1016/j.ddtec.2018.04.001.
29. K. Mioduszewska, J. Dolzonek, D. Wyrzykowski, L. Kubik, P. Wiczling, C. Sikorska, M. Tonski, Z. Kaczyński, P. Stepnowski, and A. Bialk-Bielińska, *Trend. Anal. Chem.*, **97**, 283–296 (2017), doi: 10.1016/j.trac.2017.09.009.
30. W. A. Marinaro, L. J. Schieber, E. J. Munson, V. W. Day, and V. J. Stella, *J. Pharm. Sci.*, **101**, 310–318 (2012), doi: 10.1002/jps.23207.
31. C. Liu, Q. Yin, X. Li, L. Hao, W. Zhang, Y. Bao, and J. Ma, *Adv. Comp. Hyb. Mater.*, **4**, 138–149 (2021), doi: 10.1007/s42114-021-00206-3.
32. A. Adamczyk-Woźniak, M.K. Cyrański, K. Durka, J.T. Gozdalik, P. Klimentowska, R. Rusiecki, A. Sporzyński, and D. Zarzeczańska, *Crystals.*, **9**, 109–125 (2019), doi: 10.3390/cryst9020109.
33. F. G. Der, G. Yalcin, E. Ozcan Bulbul, H. İleri, B. Cihan, M. Gokcan, Y. C. Esitmez, and E. Kilinc, *Electroanalysis*, **34**, 1711–1734 (2022), doi: 10.1002/elan.202200012.